2023 IEEE Nanotechnology Materials
and Devices Conference (NMDC)
October 22-25 2023. Paestum (Salerno), Italy

Chemistry for the Focused Electron and Ion Beam-Induced Deposition of Metal Nanostructures

Atul Chaudhary[1], Patrick Eckhert[2], D. Howard Fairbrother[2] and Lisa McElwee-White[1,*]
[1]*Department of Chemistry, University of Florida, Gainesville, Florida 32611-7200, United States*
[2]*Department of Chemistry, Johns Hopkins University, Baltimore, Maryland 21218, United States*

2023 IEEE Nanotechnology Materials and Devices Conference (NMDC) | 979-8-3503-3546-0/23/$31.00 ©2023 IEEE | DOI: 10.1109/NMDC57951.2023.10344187

***Abstract*— Focused electron beam-induced deposition (FEBID) and focused ion beam-induced deposition (FIBID) are cutting-edge nanofabrication techniques that enable the growth of complex three-dimensional (3D) nanostructures by action of the charged particles upon organometallic precursors. The interaction of the focused electron/ion beam with the adsorbed precursor molecules on the substrate surface leads to the dissociation of these surface-bound species resulting in the formation of well-defined deposits. However, during the deposition process, decomposition and incomplete desorption of the organic ligands give rise to contamination in the final deposits, reducing their metal content. To enable applications where deposit composition is critical, it will be necessary to design and synthesize custom precursors for FEBID/FIBID. UHV surface science studies can be used to understand the decomposition mechanism of the organometallic precursors during the electron- or ion-molecule interaction, generating information that can be used in mechanism-based precursor design.**

Keywords*— *FEBID, FIBID, organometallic precursors, focused ion beam (FIB)

I. Introduction

Focused electron beam-induced deposition (FEBID) and focused ion beam-induced deposition (FIBID) are single-step, direct write, maskless, nanofabrication techniques that enable the direct deposition of three-dimensional (3D) nanostructures onto both planar and non-planar substrates [1-4]. As a result, FEBID and FIBID can be utilized to fabricate intricate metal nanostructures such as nanodots, nanocubes and nanowires with precise control and accuracy, leading to industrial applications in circuit editing [5, 6] and repair of the masks used in photolithography [7-10].

Typically, FEBID is performed in a scanning electron microscope where the background pressure of the vacuum chamber is maintained at 10^{-6} mbar while steady-state delivery of gaseous organometallic precursors provides reagents for the deposition process as shown in Fig. 1. The primary focused electron beam (≥ 5 keV) interacts with the substrate, producing lower energy secondary electrons (0-100 eV). The secondary electrons play an important role in the deposition process by inducing electron-stimulated decomposition of transiently adsorbed organometallic precursor molecules on the substrate surface. The electron-molecule interaction leads to the cleavage of bonds in the precursor forming non-volatile fragments which give rise to the deposits while volatile fragments are pumped away from the system [11]. In the case of FIBID, the deposition process is more complex. While deposits can result from momentum transfers due to collision between the ions from the beam and the adsorbed precursor molecules, secondary electrons may also play a role. During FIBID, ion-induced sputtering also occurs during deposition [3, 12]. The concomitant sputtering can be an advantage in obtaining high metal content material because it will result in purification of the deposit if the impurities are preferentially removed. However, it is important to maintain a balance between the deposition and sputtering processes to obtain a deposit without etching of the metal atoms. Other complications during FIBID can include amorphization and ion implantation [13].

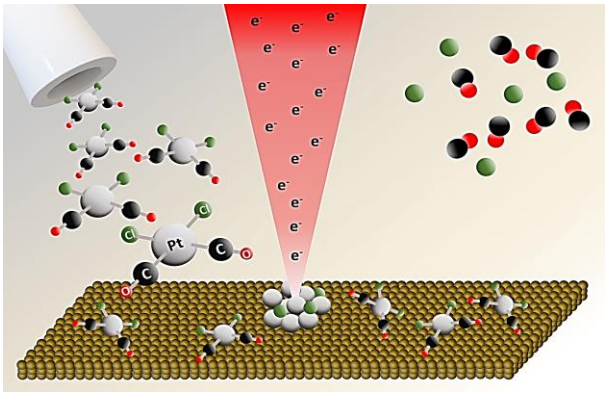

Fig. 1. Illustration of the focused electron beam-induced deposition process for cis $Pt(CO)_2(Cl)_2$. Reprinted with permission from reference [11]. Copyright 2021 American Chemical Society.

The metal content in a FEBID deposit is strongly influenced by the choice of precursor used during the deposition process. The low metal content in the FEBID/FIBID deposits is due to the partial decomposition of the organic ligands of the precursor, forming the carbonaceous matrix which affects the conductivity, plasmonic response, catalytic reactivity, and magnetic properties of the deposited material. Therefore, it is important to tailor the organometallic precursor so that its decomposition under FEBID/FIBID experimental conditions results in enhanced metal content in the final deposits. During the early development of FEBID, it was standard practice to use commercially available chemical

*Corresponding author: phone: 352-392-8768; fax: 352-846-0296; email: lmwhite@chem.ufl.edu

979-8-3503-3546-0/23/$31.00 ©2023 IEEE

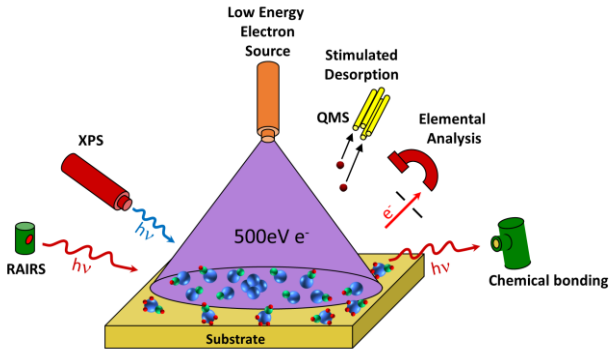

Fig. 2. Schematic representation of the ultrahigh vacuum (UHV) surface science approach to studying FEBID precursors. Reprinted with permission from reference [11]. Copyright 2021 American Chemical Society.

vapor deposition (CVD) precursors for FEBID experiments, due to their easy accessibility and known volatility. However, the CVD and FEBID processes have different mechanisms of precursor decomposition during the deposition process. The deposition in CVD is a thermal process while the precursor chemistry in FEBID/FIBID is driven by charged particle-molecule interactions. An understanding of the mechanism of charged particle-induced precursor decomposition is critical for development of tailored precursors for FEBID/FIBID [11, 14, 15].

The UHV surface science approach (Fig. 2) is a valuable method to investigate decomposition mechanisms of charged particle-induced reactions of organometallic precursors [16]. In these experiments, a few monolayers of the precursor complex are condensed on a cold substrate and subjected to electron irradiation using a flood gun or ion bombardment from an ion gun under UHV conditions (<5 x 10-9 Torr). The non-volatile decomposition products can be characterized in situ by X-ray photoelectron spectroscopy (XPS) while volatile byproducts can be analyzed by mass spectrometry (MS). The UHV studies can be used to get mechanistic and kinetic details regarding the precursor decomposition during the irradiation process, leading to closure of the feedback loop for improved design of tailored precursors for FEBID and FIBID.

II. Results and Discussion

As a part of our effort to identify a privileged set of ligands for organometallic FEBID precursors [11, 14], the ruthenium tricarbonyl allyl halide precursors (η^3-allyl)$Ru(CO)_3X$ [X = Cl, Br] (Fig. 3) which contain three different types of ligands [carbonyl (CO), allyl (η^3-C_3H_5), halide (Cl, Br)] were investigated using the UHV surface science approach to gain a deeper understanding of the electron-induced decomposition mechanism [17]. During the UHV studies, a thin film of (η^3-allyl)$Ru(CO)_3X$ [X = Cl, Br] was condensed onto a chemically inert cooled substrate and XPS analysis was performed before and after electron beam irradiation (Fig. 4). The XPS data were consistent with facile electron-induced dissociation of the carbonyl ligands, while minimal, if any, dissociation of the anionic π-facial allyl (η^3-C_3H_5) ligands occurred. Decomposition of the allyl ligands was postulated to be the source of the organic contamination in the deposits. The allyl ligand was thus ruled out as a privileged ligand for FEBID.

The bromide ligand of (η^3-allyl)$Ru(CO)_3Br$ was an interesting intermediate case for electron-induced reactivity. After extensive electron irradiation that modeled post-deposition processing after FEBID, the majority of the bromine ligands were removed upon increasing the electron dosage but it was clear that bromide dissociation was much less facile than carbonyl loss, even upon electron irradiation of only a few monolayers of precursor. Under FEBID conditions, where steady state delivery of precursor would cover the surface of the deposit, the slow loss of bromide from the surface would be expected to be problematic.

Electron-induced loss of halide ligand from the ruthenium tricarbonyl allyl halide precursors (η^3-allyl)$Ru(CO)_3X$ [X = Cl, Br] could also be facilitated by electron irradiation in the presence of NH_3 [18]. These experiments model post-deposition processing with addition of a coreactant. For the chloride complex (η^3-allyl)$Ru(CO)_3Cl$, the electron-induced reaction with NH_3

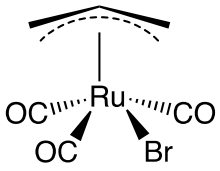

Fig. 3. Structure of (η^3-allyl)$Ru(CO)_3Br$.

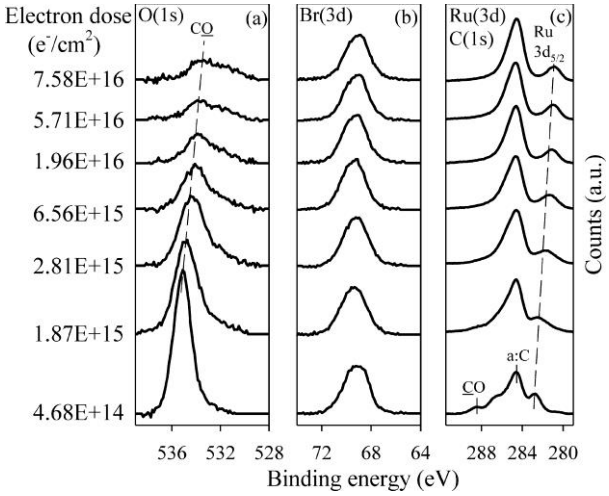

Fig. 4. Evolution of the (a) O(1s), (b) Br(3d), and (c) Ru(3d)/C(1s) XP regions for 1–2 nm thick films of [(η^3-C_3H_5)$Ru(CO)_3Br$] exposed to electron doses of ≤7.58 × 10^{16} e^-/cm^2. Spectral intensities were normalized to compensate for slight differences in film thickness between samples. Reprinted with permission from reference [17]. Copyright 2015 American Chemical Society.

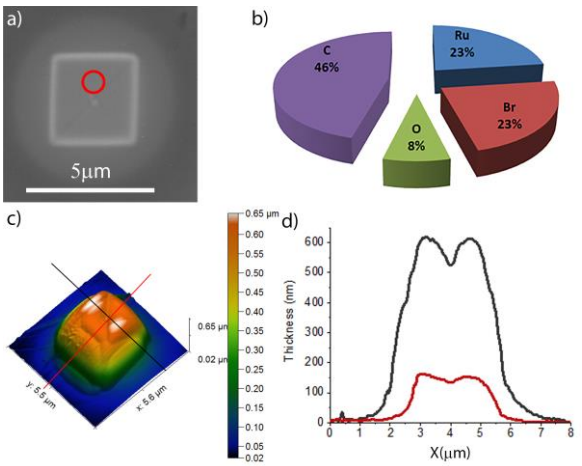

Fig. 5 (a) Top-view scanning electron micrograph of a typical 3 × 3 μm deposit on a native oxide Si substrate with the red circle symbolizing the EDX and WDS measurement area, with excitation range. (b) Average composition of the deposit (in at. %, with uncertainty approximately 3 at. %). (c) AFM 3D measurement of the shape of the deposit before purification. (d) AFM profiles measured through the center of the deposit before (black) and after (red) purification by annealing at 300 °C under forming gas. Red and black lines in (c) are the line profile positions for part (d). Reprinted with permission from reference [19]. Copyright 2019 American Chemical Society.

resulted in loss of Cl as the volatile byproduct HCl. After multiple cycles of condensation of NH_3 followed by electron exposure and annealing, the Cl content of the film could be reduced by up to 75%. However, the carbon from the allyl ligand remained in the solid.

FEBID studies on (η^3-C_3H_5)$Ru(CO)_3Br$ produced 3D structures that were 23 at% Ru, with the remaining material composed of C, Br and O residue from the ligands (Fig. 5) [19]. The deposits could be purified to 83 at% Ru by annealing at 300 °C in an atmosphere of 2% H_2 in N_2. After purification, the bromine content was below detectable limits and the carbon impurities predominantly derived from the allyl ligand had been reduced to 13 at%, as measured using EDS and WDS.

These studies on the electron-induced reactivity of (η^3-allyl)$Ru(CO)_3Br$ in the presence and absence of coreactants and experiments on postdeposition processing led to the conclusion that smaller ligands such as carbonyls and halides are promising choices for the set of privileged ligands for FEBID, while the anionic π-facial allyl (η^3-C_3H_5) ligand was not suitable. The feedback loop to precursor design resulted in investigations of $Ru(CO)_4X_2$ [X = Br, I] that contained only halide and carbonyl ligands.

In order to study charged-particle induced reactivity of organometallic precursors that have only carbonyl and halide ligands, UHV surface science studies were performed with $Ru(CO)_4I_2$ and $Ru(CO)_4Br_2$ [20]. In these experiments, irradiation of a thin film of $Ru(CO)_4I_2$ on Au with electrons at 500 eV resulted in rapid loss of two CO ligands, which gives rise to a partially decarbonylated Ru iodide species. This intermediate species then undergoes a slower step in which the remaining two CO ligands are desorbed, leaving a deposit containing ruthenium and iodine. The behavior of the bromide complex $Ru(CO)_4Br_2$ was similar, ultimately affording a deposit composed of ruthenium and bromine after extensive electron exposure (Fig. 6).

The inability of electron exposure to remove the halides from $Ru(CO)_4I_2$ and $Ru(CO)_4Br_2$ under UHV conditions, led to exploration of ion-induced chemistry of $Ru(CO)_4I_2$ [21]. FIBID can achieve higher metal contents than FEBID in deposits from organometallic precursors due to the competition between deposition and sputtering that can selectively remove impurities (*vide supra*). As a consequence, UHV surface science studies were also performed in which thin films of $Ru(CO)_4I_2$ were subjected to ion bombardment with low energy Ar^+ (860

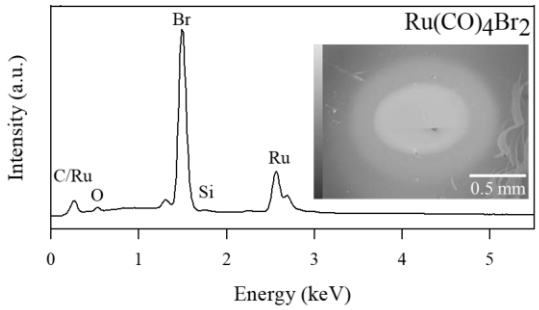

Fig. 6. EDS spectrum of a deposit made by EBID from $Ru(CO)_4Br_2$ under UHV conditions. To the right of the spectrum is an SEM image of the deposit. Reprinted with permission from reference [20]. Copyright 2020 American Chemical Society.

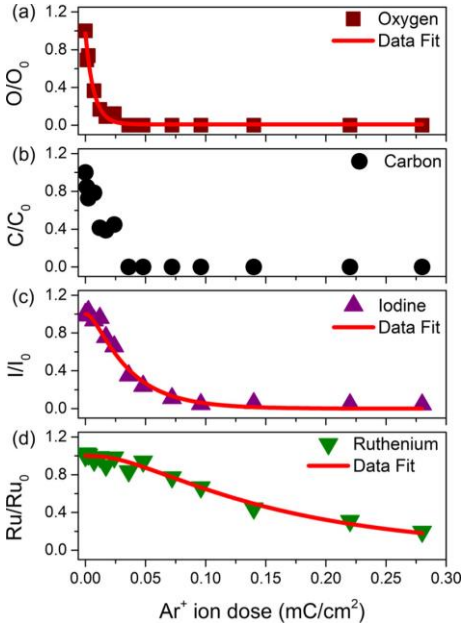

Fig. 7. Change in fractional coverage of O, C, I, and Ru atoms as a function of increasing Ar^+ dose. Ratios were obtained from XPS of ≈ 1.6-1.7 nm films of $Ru(CO)_4I_2$ adsorbed onto a Au substrate at -100 °C and exposed to increasing dose of Ar^+ ions. The graphs (a,c,d) were fit by integrated rate functions. Reprinted with permission from reference [21]. Copyright 2020 American Chemical Society.

V). The ion-induced reactions resulted in the desorption of all four CO ligands as a result of energy transfer from the incident ions. A slower sputtering process preferentially removes iodine atoms, eventually affording a deposit of Ru metal (Fig. 7). These studies allowed comparison of electron- and ion-induced reactivity under the UHV surface science conditions used to model FEBID/FIBID. Under ion bombardment, $Ru(CO)_4I_2$ underwent rapid loss of all four CO ligands followed by slower sputtering to afford Ru metal while electron exposure resulted in rapid loss of two CO ligands followed by slower loss of two more to ultimately give a deposit of RuI_2.

III. Conclusion

Mechanism-based tailoring of organometallic precursors for FEBID and FIBID will be important for enabling use of these fabrication techniques in applications where the composition of the deposit is critical. Because impurities in the deposits are largely derived from fragments of ligands that decompose but do not desorb from the deposit surface, identifying a set of privileged ligands that preferentially undergo dissociation over decomposition during the charged particle-molecule interaction will enable precursor design. To that end, we have identified CO ligands as belonging to the privileged class. Halide ligands are also possibilities as privileged ligands but coreactants could be required for their use. Anionic π-facial ligands are apparently ruled out. Continuing to use the UHV surface science approach to investigate the electron- and ion-stimulated reactions of adsorbed precursors will allow elucidation of their kinetic and mechanistic details. The resulting structure-activity relationships of the precursors will ultimately enable the control over the composition of fabricated materials for the desired applications.

ACKNOWLEDGMENT

LMW and DHF thank the National Science Foundation for support of this work through the linked collaborative grants CHE-1607621, CHE-1904559 and CHE-1607547, CHE-1904802. We thank Xin Kang and Dr. Jo-Chi Yu for assistance with precursor synthesis. We also thank our collaborators supported within the frameworks of MultIChem and FIT4NANO, European Union Horizon 2020 research and innovation programs under COST Action numbers CA20129 and CA19140

REFERENCES

[1] I. Utke and A. Golzhauser, "Small, Minimally Invasive, Direct: Electrons Induce Local Reactions of Adsorbed Functional Molecules on the Nanoscale," (in English), *Angew. Chem. Int. Ed.,* vol. 49, no. 49, pp. 9328-9330, 2010, doi: DOI 10.1002/anie.201002677.

[2] M. Huth, F. Porrati, and O. V. Dobrovolskiy, "Focused Electron Beam Induced Deposition Meets Materials Science," *Microelectron. Eng.,* vol. 185-186, pp. 9-28, 2018/01/05/ 2018, doi: 10.1016/j.mee.2017.10.012.

[3] I. Utke, P. Hoffmann, and J. Melngailis, "Gas-assisted Focused Electron Beam and Ion Beam Processing and Fabrication," *J. Vac. Sci. Technol., B,* vol. 26, no. 4, pp. 1197-1276, 2008, doi: 10.1116/1.2955728.

[4] M. Huth *et al.*, "Focused Electron Beam Induced Deposition: A Perspective," (in eng), *Beilstein J. Nanotech.,* vol. 3, pp. 597-619, 2012, doi: 10.3762/bjnano.3.70.

[5] I. Utke, S. Moshkalev, and P. Russell, *Nanofabrication Using Focused Ion and Electron Beams: Principles and Applications*. Oxford University Press, 2012.

[6] R. Córdoba, P. Orús, S. Strohauer, T. E. Torres, and J. M. De Teresa, "Ultra-fast Direct Growth of Metallic Micro-and Nano-Structures by Focused Ion Beam Irradiation," *Sci. Rep.,* vol. 9, no. 1, pp. 1-10, 2019, doi: 10.1038/s41598-019-50411-w

[7] K. Edinger *et al.*, "Electron-beam-based photomask repair," *J. Vac. Sci. Technol. B,* vol. 22, no. 6, pp. 2902-2906, 2004, doi: 10.1116/1.1808711.

[8] T. Liang, E. Frendberg, B. Lieberman, and A. Stivers, "Advanced Photolithographic Mask Repair Using Electron Beams," *J. Vac. Sci. Technol. B,* vol. 23, no. 6, pp. 3101-3105, 2005, doi: 10.1116/1.2062428.

[9] C. T. H. Heerkens, M. Kamerbeek, W. van Dorp, C. Hagen, and J. Hoekstra, "Electron Beam Induced Deposited Etch Masks," *Microelectron. Eng.,* vol. 86, no. 4, pp. 961-964, 2009, doi: 10.1016/j.mee.2008.11.079.

[10] T. Bret, T. Hofmann, and K. Edinger, "Industrial perspective on focused electron beam-induced processes," *Appl. Phys. A,* journal article vol. 117, no. 4, pp. 1607-1614, December 01 2014, doi: 10.1007/s00339-014-8601-2.

[11] J.-C. Yu, M. K. Abdel-Rahman, D. H. Fairbrother, and L. McElwee-White, "Charged Particle-Induced Surface Reactions of Organometallic Complexes as a Guide to Precursor Design for Electron- and Ion-Induced Deposition of Nanostructures," *ACS Appl. Mater. Interfaces,* vol. 13, no. 41, pp. 48333-48348, 2021, doi: 10.1021/acsami.1c12327.

[12] K. Höflich *et al.*, "Roadmap for focused ion beam technologies," *arXiv:2305.19631*.

[13] Y. Drezner, D. Fishman, Y. Greenzweig, and A. Raveh, "Characterization of damage induced by FIB etch and tungsten deposition in high aspect ratio vias," *J. Vac. Sci. Technol. B,* vol. 29, no. 1, p. 011026, 2011.

[14] W. G. Carden, H. Lu, J. A. Spencer, D. H. Fairbrother, and L. McElwee-White, "Mechanism-Based Design of Precursors for Focused Electron Beam-Induced Deposition," *MRS Commun.,* vol. 8, no. 2, pp. 343-357, 2018, doi: 10.1557/mrc.2018.77.

[15] S. Barth, M. Huth, and F. Jungwirth, "Precursors for Direct-Write Nanofabrication With Electrons," *J. Mater. Chem. C,* vol. 8, no. 45, pp. 15884-15919, Dec 2020, doi: 10.1039/d0tc03689g.

[16] J. A. Spencer, S. G. Rosenberg, M. Barclay, Y.-C. Wu, L. McElwee-White, and D. H. Fairbrother, "Understanding the Electron-Stimulated Surface Reactions of Organometallic Complexes to Enable Design of Precursors for Electron Beam-Induced Deposition," *Appl. Phys. A,* vol. 117, no. 4, pp. 1631-1644, 2014/12// 2014, doi: 10.1007/s00339-014-8570-5.

[17] J. A. Spencer, J. A. Brannaka, M. Barclay, L. McElwee-White, and D. H. Fairbrother, "Electron-Induced Surface Reactions of η^3-Allyl Ruthenium Tricarbonyl Bromide $[(\eta^3\text{-}C_3H_5)Ru(CO)_3Br]$: Contrasting the Behavior of Different Ligands," *J. Phys. Chem. C,* vol. 119, no. 27, pp. 15349-15359, 2015, doi: 10.1021/acs.jpcc.5b03775.

[18] M. Rohdenburg, H. Boeckers, C. R. Brewer, L. McElwee-White, and P. Swiderek, "Efficient NH_3-based process to remove chlorine from electron beam deposited ruthenium produced from $(\eta^3\text{-}C_3H_5)Ru(CO)_3Cl$," *Sci. Rep.,* vol. 10, no. 1, p. 10901, Jul 2020, doi: 10.1038/s41598-020-67803-y.

[19] J. Jurczyk *et al.*, "Focused electron beam induced deposition and post-growth purification using the heteroleptic Ru complex $(\eta^3\text{-}C_3H_5)Ru(CO)_3Br$," *ACS Appl. Mater. Interfaces,* vol. 11, pp. 28164-28171, 2019, doi: 10.1021/acsami.9b07634.

[20] R. M. Thorman *et al.*, "Electron-Induced Reactions of $Ru(CO)_4I_2$: Gas Phase, Surface, and Electron Beam-Induced Deposition," *J. Phys. Chem. C,* vol. 124, no. 19, pp. 10593-10604, May 2020, doi: 10.1021/acs.jpcc.0c01801.

[21] E. Bilgilisoy *et al.*, "Surface Reactions of Low-Energy Argon Ions with Organometallic Precursors," *J. Phys. Chem. C,* vol. 124, pp. 24795-24808, 2020/10/30 2020, doi: 10.1021/acs.jpcc.0c07269.